Resonance Frequency, Gain, Efficiency and Quality Factor of a Microstrip Printed Antenna as a Function of Curvature for TM_{01} mode Using Different Substrates

Ali Elrashidi[1], Khaled Elleithy[2], Hassan Bajwa [3]

[1]Department of Computer and Electrical Engineering, University of Bridgeport, Bridgeport, CT 06604, USA (aelrashi@bridgeport.edu)
2Department of Computer and Electrical Engineering, University of Bridgeport, Bridgeport, CT 06604, USA (elleithy@bridgeport.edu)
3Department of Computer and Electrical Engineering, University of Bridgeport, Bridgeport, CT 06604, USA (hbjwa@bridgeport.edu)

Abstract Curvature has an important effect on fringing field of a microstrip antenna and consequently fringing field affects the effective dielectric constant and then all antenna parameters. A new mathematical model for resonance frequency, gain, efficiency and quality factor as a function of curvature is introduced in this paper. These parameters are given for TM_{01} mode and using three different substrate materials RT/duroid-5880 PTFE, K-6098 Teflon/Glass and Epsilam-10 ceramic-filled Teflon.

Keywords Fringing field, curvature, effective dielectric constant, gain, efficiency, Q-factor, and Transverse Magnetic TM_{01} mode.

1. Introduction

Due to the unprinted growth in wireless applications and increasing demand of low cost solutions for RF and microwave communication systems, the microstrip flat antenna, has undergone tremendous growth recently. Though the models used in analyzing microstrip structures have been widely accepted, the effect of curvature on dielectric constant and antenna performance has not been studied in detail. Low profile, low weight, low cost and its ability of conforming to curve surfaces [1], conformal microstrip structures have also witnessed enormous growth in the last few years. Applications of microstrip structures include Unmanned Aerial Vehicle (UAV), planes, rocket, radars and communication industry [2]. Some advantages of conformal antennas over the planer microstrip structure include, easy installation (randome not needed), capability of embedded structure within composite aerodynamic surfaces, better angular coverage and controlled gain, depending upon shape [3, 4]. While Conformal Antenna provide potential solution for many applications, it has some drawbacks due to bedding [5]. Such drawbacks include phase, impedance, and resonance frequency errors due to the stretching and compression of the dielectric material along the inner and outer surfaces of conformal surface. Changes in the dielectric constant and material thickness also affect the performance of the antenna. Analysis tools for conformal arrays are not mature and fully developed [6]. Dielectric materials suffer from cracking due to bending and that will affect the performance of the conformal microstrip antenna.

2. Background

Conventional microstrip antenna has a metallic patch printed on a thin, grounded dielectric substrate. Although the patch can be of any shape, rectangular patches, as shown in Figure 1 [7], are preferred due to easy calculation and modeling.

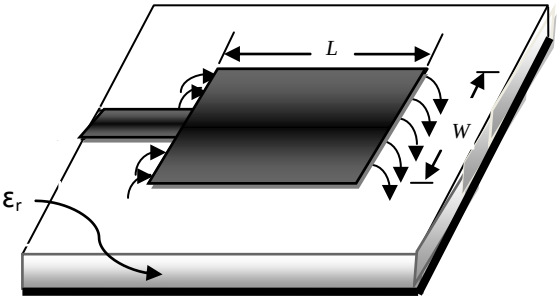

Figure 1. Rectangular microstrip antenna

Fringing fields have a great effect on the performance of a microstrip antenna. In microstrip antennas the electric filed in the center of the patch is zero. The radiation is due to the fringing field between the periphery of the patch and the ground plane. For the rectangular patch shown in the Figure 2, there is no field variation along the width and thickness. The amount of the fringing field is a function of the dimensions of the patch and the height of the substrate. Higher the substrate, the greater is the fringing field.

Due to the effect of fringing, a microstrip patch antenna would look electrically wider compared to its physical dimensions. As shown in Figure 2, waves travel both in substrate and in the air. Thus an effective dielectric constant

ε_{reff} is to be introduced. The effective dielectric constant ε_{reff} takes in account both the fringing and the wave propagation in the line.

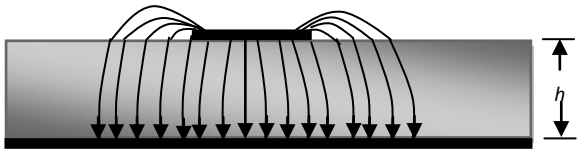

Figure 2. Electric field lines (Side View).

The expression for the effective dielectric constant is introduced by A. Balanis [7], as shown in Equation 1.

$$\varepsilon_{reff} = \frac{\varepsilon_r + 1}{2} + \frac{\varepsilon_r - 1}{2}\left[1 + 12\frac{h}{w}\right]^{-\frac{1}{2}} \quad (1)$$

The length of the patch is extended on each end by ΔL is a function of effective dielectric constant ε_{reff} and the width to height ratio (W/h). ΔL can be calculated according to a practical approximate relation for the normalized extension of the length [8], as in Equation 2.

$$\frac{\Delta L}{h} = 0.412\frac{(\varepsilon_{reff} + 0.3)\left(\frac{W}{h} + 0.264\right)}{(\varepsilon_{reff} - 0.258)\left(\frac{W}{h} + 0.8\right)} \quad (2)$$

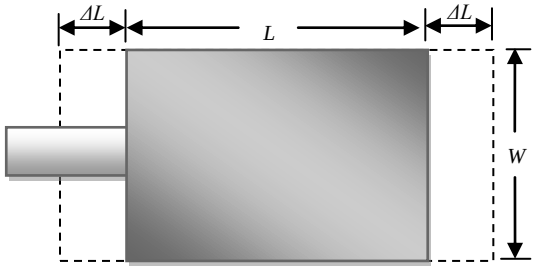

Figure 3. Physical and effective lengths of rectangular microstrip patch.

The effective length of the patch is L_{eff} and can be calculated as in Equation 3.

$$L_{eff} = L + 2\Delta L \quad (3)$$

By using the effective dielectric constant (Equation 1) and effective length (Equation 3), we can calculate the resonance frequency of the antenna f and all the microstrip antenna parameters.

Cylindrical-Rectangular Patch Antenna

All the previous work for a conformal rectangular microstrip antenna assumed that the curvature does not affect the effective dielectric constant and the extension on the length. The effect of curvature on the resonant frequency has been presented previously [9]. In this paper we present the effect of fringing field on the performance of a conformal patch antenna. A mathematical model that includes the effect of curvature on fringing field and on antenna performance is presented. The cylindrical rectangular patch is the most famous and popular conformal antenna. The manufacturing of this antenna is easy with respect to spherical and conical antennas.

Effect of curvature of conformal antenna on resonant frequency been presented by Clifford M. Krowne [9, 10] as:

$$[(f]_r)_{mn} = \frac{1}{2\sqrt{\mu\varepsilon}}\sqrt{\left(\frac{m}{2\theta a}\right)^2 + \left(\frac{n}{2b}\right)^2} \quad (4)$$

Where $2b$ is a length of the patch antenna, a is a radius of the cylinder, 2θ is the angle bounded the width of the patch, ε represents electric permittivity and μ is the magnetic permeability as shown in Figure 4.

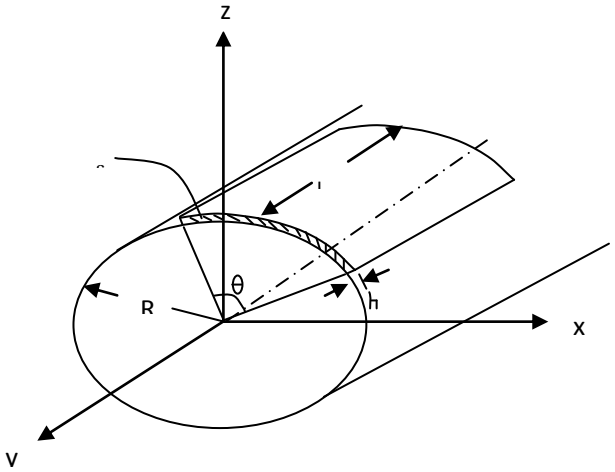

Figurer 4. Geometry of cylindrical-rectangular patch antenna[9]

Joseph A. *et al*, presented an approach to the analysis of microstrip antennas on cylindrical surface. In this approach, the field in terms of surface current is calculated, while considering dielectric layer around the cylindrical body. The assumption is only valid if radiation is smaller than stored energy[11]. Kwai *et al*. [12]gave a brief analysis of a thin cylindrical-rectangular microstrip patch antenna which includes resonant frequencies, radiation patterns, input impedances and Q factors. The effect of curvature on the characteristics of TM_{10} and TM_{01} modes is also presented in Kwai *et al*. paper. The authors first obtained the electric field under the curved patch using the cavity model and then calculated the far field by considering the equivalent magnetic current radiating in the presence of cylindrical surface. The cavity model, used for the analysis is only valid for a very thin dielectric. Also, for much small thickness than a wavelength and the radius of curvature, only *TM* modes are assumed to exist. In order to calculate the radiation patterns of cylindrical-rectangular patch antenna. The authors introduced the exact Green's function approach. Using Equation (4), they obtained expressions for the far zone electric field components E_θ and E_φ as a functions of Hankel function of the second kind $H_p^{(2)}$. The input impedance and Q factors are also calculated under the same conditions.

Based on cavity model, microstrip conformal antenna on a projectile for GPS (Global Positioning System) device is designed and implemented by using perturbation theory is introduced by Sun L., Zhu J., Zhang H. and Peng X [13].

The designed antenna is emulated and analyzed by IE3D software. The emulated results showed that the antenna could provide excellent circular hemisphere beam, better wide-angle circular polarization and better impedance match peculiarity.

Nickolai Zhelev introduced a design of a small conformal microstrip GPS patch antenna [14]. A cavity model and transmission line model are used to find the initial dimensions of the antenna and then electromagnetic simulation of the antenna model using software called FEKO is applied. The antenna is experimentally tested and the author compared the result with the software results. It was founded that the resonance frequency of the conformal antenna is shifted toward higher frequencies compared to the flat one.

The effect of curvature on a fringing field and on the resonance frequency of the microstrip printed antenna is studied in [15]. Also, the effect of curvature on the performance of a microstrip antenna as a function of temperature for TM_{01} and TM_{10} is introduced in [16], [17].

3. General Expressions for Electric and Magnetic Fields Intensities

In this section, we will introduce the general expressions of electric and magnetic field intensities for a microstrip antenna printed on a cylindrical body represented in cylindrical coordinates.
Starting from Maxwell's Equations, we can get the relation between electric field intensity *E* and magnetic flux density *B* as known by Faraday's law [18], as shown in Equation (2):

$$\nabla \times E = -\frac{\partial B}{\partial t} \tag{2}$$

Magnetic field intensity *H* and electric flux density *D* are related by Ampérés law as in Equation (3):

$$\nabla \times H = J + \frac{\partial D}{\partial t} \tag{3}$$

where *J* is the electric current density.

The magnetic flux density *B* and electric flux density *D* as a function of time *t* can be written as in Equation (4):

$$B(t) = \mu\, H\, e^{-j\omega t} \quad \text{and} \quad D(t) = \varepsilon\, E\, e^{-j\omega t} \tag{4}$$

where μ is the magnetic permeability and ε is the electric permittivity.
By substituting Equation (4) in Equations (2) and (3), we can get:

$$\nabla \times E = -j\omega\mu \mathrm{H} \quad \text{and} \quad \nabla \times H = j\omega\varepsilon E + J \tag{5}$$

where ω is the angular frequency and has the form of: $\omega = 2\pi f$. In homogeneous medium, the divergence of Equation (2) is:

$$\nabla . H = 0 \quad \text{and} \quad H = \nabla \times A \tag{6}$$

From Equation (5), we can get Equation (7):

$$\nabla \times E + j\omega\mu \mathrm{H} = 0 \quad \text{or} \quad \nabla \times (E + j\omega\mu \mathrm{A}) = 0 \tag{7}$$

Using the fact that, any curl free vector is the gradient of the same scalar, hence:

$$(E + j\omega\mu \mathrm{A}) = -\nabla\varphi \tag{8}$$

where φ is the electric scalar potential.

By letting: $\nabla . A = -j\omega\mu\varphi$

where *A* is the magnetic vector potential.
So, the Helmholtz Equation takes the form of (9):

$$\nabla^2 \mathrm{A} + k^2 = -\mathrm{J} \tag{9}$$

k is the wave number and has the form of: $k = \omega\sqrt{\mu\varepsilon}$, and ∇^2 is Laplacian operator. The solutions of Helmholtz Equation are called wave potentials:

$$E = -j\omega\mu\varepsilon A + \frac{1}{j\omega\varepsilon}\nabla(\nabla . \mathrm{A}) \tag{10}$$

$$H = \nabla \times A$$

3.1 Near Field Equations

By using the Equations number (10) and magnetic vector potential in [19], we can get the near electric and magnetic fields as shown below:

$$E_z = \frac{1}{2\pi j\omega\varepsilon} \sum_{n=-\infty}^{\infty} e^{jn\emptyset} \int_{-\infty}^{\infty} (k^2 - k_z^2) f_n(k_z) H_n^{(2)}\left(\rho\sqrt{k - k_z^2}\right) e^{jk_z z}\, dk_z \tag{12}$$

E_φ and E_ρ are also getting using Equation (7);

$$E_\emptyset = -\frac{1}{2\pi j\omega\varepsilon} \sum_{n=-\infty}^{\infty} e^{jn\emptyset} \int_{-\infty}^{\infty} k_z f_n(k_z) H_n^{(2)}\left(\rho\sqrt{k - k_z^2}\right) e^{jk_z z}\, dk_z \tag{13}$$

$$E_\rho = \frac{1}{2\pi j\omega\varepsilon} \sum_{n=-\infty}^{\infty} e^{jn\emptyset} \int_{-\infty}^{\infty} \sqrt{k^2 - k_z^2} f_n(k_z) H_n^{(2)'}\left(\rho\sqrt{k - k_z^2}\right) e^{jk_z z}\, dk_z \tag{14}$$

To get the magnetic field in all directions, we can use the second part of Equation (10) as shown below, where $H_z = 0$ for *TM* mode:

$$H_\emptyset = \frac{\partial\psi}{\partial\emptyset} = \frac{j}{2\pi} \sum_{n=-\infty}^{\infty} n e^{jn\emptyset} \int_{-\infty}^{\infty} f_n(k_z) H_n^{(2)}\left(\rho\sqrt{k - k_z^2}\right) e^{jk_z z}\, dk_z \tag{15}$$

$$H_\rho = -\frac{\partial \psi}{\partial \rho} = -\frac{1}{2\pi}\sum_{n=-\infty}^{\infty}\int_{-\infty}^{\infty} f_n(k_z)\sqrt{k^2-k_z^2}H_n^{(2)'}\left(\rho\sqrt{k-k_z^2}\right)e^{jn\emptyset}\, e^{jk_z z}\, dk_z \quad (16)$$

3.2 Far Field Equations

In case of far field, we need to represent the electric and magnetic field in terms of *r*, where *r* is the distance from the center to the point that we need to calculate the field on it. By using the cylindrical coordinate Equations, one can notice that a far field ρ tends to infinity when *r*, in Cartesian coordinate, tends to infinity. Also, using simple vector analysis, one can note that, the value of k_z will equal to $-k \times cos\theta$ [19], and from the characteristics of Hankel function, we can rewrite the magnetic vector potential illustrated in Equation (12) to take the form of far field as illustrated in Equation (17).

$$A_z \xrightarrow{r\to\infty} \frac{e^{-jkr}}{\pi r}\sum_{n=-\infty}^{\infty} e^{jn\emptyset} j^{n+1} f_n(-kcos\theta) \quad (17)$$

Hence, the electric and magnetic field can easily be calculated as shown below:

$$E_z = \frac{e^{-jkr}}{j\omega\varepsilon\pi r} k^2 \sum_{n=-\infty}^{\infty} e^{jn\emptyset} j^{n+1} f_n(-kcos\theta) \quad (18)$$

$$E_\emptyset = \frac{e^{-jkr}}{j\omega\varepsilon\pi r}\sum_{n=-\infty}^{\infty} jn\, e^{jn\emptyset} j^{n+1} f_n(-kcos\theta) \quad (19)$$

$$E_r = \frac{e^{-jkr}(1+jkr)}{j\omega\varepsilon\pi r^2}\sum_{n=-\infty}^{\infty} e^{jn\emptyset} j^{n+1} f_n(-kcos\theta) \quad (20)$$

The magnetic field intensity also obtained as shown below, where $H_z = 0$:

$$H_r = \frac{e^{-jkr}(1+jkr)}{r^2}\sum_{n=-\infty}^{\infty} e^{jn\emptyset} j^{n+1} f_n(-kcos\theta) \quad (21)$$

$$H_\emptyset = \frac{-e^{-jkr}}{\pi r}\sum_{n=-\infty}^{\infty} n\, e^{jn\emptyset} j^{n+2} f_n(-kcos\theta) \quad (22)$$

4. Quality Factor, Gain, and Efficiency

Quality factor, gain, and efficiency are antenna figures-of-merit, which are interrelated, and there is no complete freedom to independently optimize each one [7].

4.1 Quality Factor

The quality factor is a figure-of-merit that is representative of the antenna losses. Typically there are radiation, conduction, dielectric and surface wave losses. Therefore the total quality factor Q_t is influenced by all of these losses and is written as:

$$\frac{1}{Q_t} = \frac{1}{Q_{rad}} + \frac{1}{Q_c} + \frac{1}{Q_d} + \frac{1}{Q_{sw}} \quad (23)$$

where
Q_t = total quality factor
Q_{rad} = quality factor due to radiation (space wave) losses
Q_c = quality factor due to conduction (ohmic) losses
Q_d = quality factor due to dielectric losses
Q_{sw} = quality factor due to surface wave losses
Q for any of the quantity on the right-hand side can be represented as:

$$Q = \frac{\omega_r W_T}{Associated\ power\ loss} \quad (24)$$

where, the stored energy at resonance W_T is the same, independent of the mechanism of power loss. Therefore, Equation (23) can be expressed as:

$$\frac{1}{Q_t} = \frac{P_d + P_c + P_r + P_{sw}}{\omega_r W_T} \quad (25)$$

The stored energy is determined by the field under the patch, and is expressed as [20]:

$$W_T = \frac{\epsilon_0\epsilon_r}{2}\iiint |E_\rho|^2 dV \quad (26)$$

We can get the electric field under the patch using Equation (14):

$$E_\rho(z,\emptyset) = \sum_n \sum_m A_{nm}\sqrt{\frac{\varepsilon_m\varepsilon_n}{2a\theta_1 L}}\cos\left(\frac{m\pi}{2\theta_1}(\emptyset - \emptyset_1)\right)\cos\left(\frac{n\pi}{L}z\right) \quad (27)$$

So the total energy stored is determined by substitute Equation (27) in Equation (26) as follow:

$$W_T = \frac{\epsilon_0\epsilon_r}{2}\sum_n\sum_m A_{nm}^2\frac{\varepsilon_m\varepsilon_n h}{2a\theta_1 L}\int_0^L\int_{-\theta_1}^{\theta_1}\int_a^{a+h}\cos^2\left(\frac{m\pi}{2\theta_1}(\emptyset - \emptyset_1)\right)\cos^2\left(\frac{n\pi}{L}z\right)d\rho d\emptyset dz \quad (28)$$

By solving this Equation, one can get the following:

$$W_T = \frac{\epsilon_0\epsilon_r}{2}$$

$$\sum_n\sum_m A_{nm}^2\frac{\varepsilon_m\varepsilon_n h}{4a}\left[1 + \frac{1}{2m\pi}\sin\left(\frac{m\pi}{\theta_1}(\theta_1 - \emptyset_1)\right) + \frac{1}{2m\pi}\sin\left(\frac{m\pi}{\theta_1}(\theta_1 + \emptyset_1)\right)\right] \quad (29)$$

The dielectric loss is calculated from the dielectric field under the patch as in [20]:

$$P_d = \frac{\omega\epsilon_0\epsilon_r tan\delta}{2}\iiint |E_\rho|^2 dV \quad (30)$$

or as a function of total energy as:

$$P_d = \omega . tan\delta\, . W_T \quad (31)$$

where *tan(δ)* is the loss tangent of the dielectric material. So; the dielectric loss is calculated using Equations (29) and (31). The power loss due to the conduction is calculated from the magnetic field on the patch metallization and ground plate,

$$P_c = R_s \iint \left|H_{surface}\right|^2 dS \tag{32}$$

where R_s is the surface resistivity of the conductors given by $\sqrt{\pi f \mu \sigma}$ and σ is the conductivity of the conductor. By using the approximation in [19] for the electric and magnetic field $E = \sqrt{\frac{\mu}{\varepsilon}} H$, and by using the height equal to *h*, one can get the following approximate Equation:

$$P_c \approx \frac{\omega . W_T}{h\sqrt{\pi f \mu \sigma}} \tag{33}$$

For very thin substrate, which is the case, the losses due to surface wave are very small and can be neglected [7]. The power radiated from the patch P_r can be determined by integrating the radiation field over the hemisphere above the patch. This is,

$$P_r = \frac{1}{2\sqrt{\frac{\mu_0}{\varepsilon_0}}} \int_0^{2\pi} \int_0^{2\pi} (|E_\theta|^2 + |E_\emptyset|^2) r^2 sin\theta \, d\theta d\emptyset \tag{34}$$

By using Equations (13)-(14), we can get an expression for E_θ and E_φ as shown below:

$$E_\emptyset = \frac{e^{-jkr}}{j\omega\varepsilon\pi r} \sum_{n=-\infty}^{\infty} jn \, e^{jn\emptyset} j^{n+1} f_n(-kcos\theta) \tag{35}$$

$$E_\theta = j\omega\mu \frac{e^{-jkr}}{\pi r} \sin\theta \sum_{n=-\infty}^{\infty} e^{jn\emptyset} j^{n+1} f_n(-kcos\theta) \tag{36}$$

Now the radiated power will take the form:

$$P_r = \frac{1}{2\sqrt{\frac{\mu_0}{\varepsilon_0}}} \int_0^{2\pi} \int_0^{2\pi} \left(\left| \frac{e^{-jkr}}{\omega\varepsilon\pi} \sum_{n=-\infty}^{\infty} n \, e^{jn\emptyset} j^{n+1} f_n(-kcos\theta) \right|^2 + \left| \omega\mu \left(\frac{e^{-jkr}}{\omega\varepsilon\pi}\right) \sin\theta \sum_{n=-\infty}^{\infty} e^{jn\emptyset} j^{n+1} f_n(-kcos\theta) \right|^2 \right) sin\theta \, d\theta d\emptyset \tag{37}$$

4.2 Antenna Gain

The gain is the ratio of the output power for an antenna to the total input power to the antenna. The input power to the antenna is the total power including, radiated power and the overall losses power. So, the gain can be represented as follows:

$$G = \frac{P_{out}(output\ power\ of\ the\ antenna)}{P_{total}(input\ power\ of\ the\ antenna)} \tag{38}$$

4.3 Antenna Efficiency

Antenna efficiency is defined as the ratio of the total radiated power to the total input power. The input power to the antenna is the total power including, radiated power and the overall losses power. So, the gain can be represented as follows:

$$\eta = \frac{P_{rad}(radiated\ power\ of\ the\ antenna)}{P_{total}(total\ input\ power\ of\ the\ antenna)} \tag{39}$$

The total input power includes the power lost due to conduction, dielectric and surface wave losses and the radiated power from the antenna.

5. Results

For the range of GHz, the dominant mode is TM_{10} for $h<<W$ which is the case. Also, for the antenna operates at the ranges 2.49, 2.24 and 1.11 GHz for three different substrates we can use the following dimensions; the original length is 41.5 cm, the width is 50 cm and for different lossy substrate we can get the effect of curvature on the effective dielectric constant and the resonance frequency.

Three different substrate materials RT/duroid-5880 PTFE, K-6098 Teflon/Glass and Epsilam-10 ceramic-filled Teflon are used for verifying the new model. The dielectric constants for the used materials are 2.2, 2.5 and 10 respectively with a tangent loss 0.0015, 0.002 and 0.004 respectively.

5.1 RT/duroid-5880 PTFE Substrate

The mathematical and experimental results for input impedance, real and imaginary parts, VSWR and return loss for a different radius of curvatures are given in [15].

Normalized electric field for different radius of curvatures is illustrated in Figure 5. Normalized electric field is plotted for θ from zero to 2π and φ equal to zero. As the radius of curvature is decreasing, the radiated electric field is getting wider, so electric field at 20 mm radius of curvature is wider than 65 mm and 65 mm is wider than flat antenna. Electric field strength is increasing with decreasing the radius of curvature, because a magnitude value of the electric field is depending on the effective dielectric constant and the effective dielectric constant depending on the radius of curvature which decreases with increasing the radius of curvature.

Normalized magnetic field is wider than normalized electric field, and also, it is increasing with deceasing radius of curvature. Obtained results are at for θ from zero to 2π and φ equal to zero and for radius of curvature 20, 65 mm and for a flat microstrip printed antenna are shown in Figure 6. For different radius of curvature, the resonance frequency changes according to the change in curvature, so the given normalized electric and magnetic fields are calculated for different resonance frequency according to radius of curvatures.

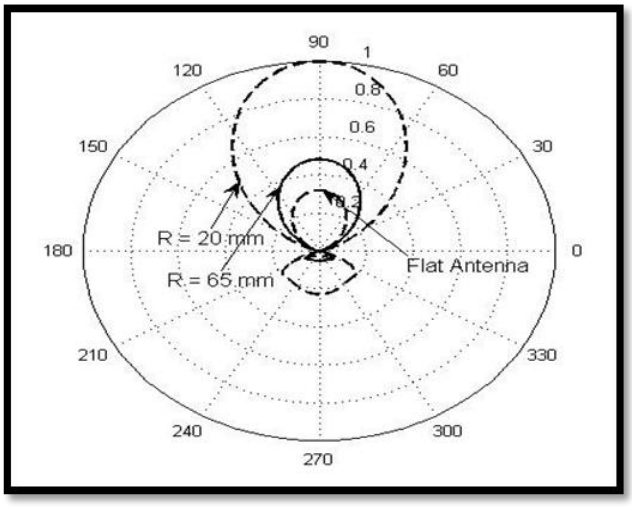

Figure 5. Normalized electric field for radius of curvatures 20, 65 mm and a flat antenna at θ=0:2π and φ=0^0.

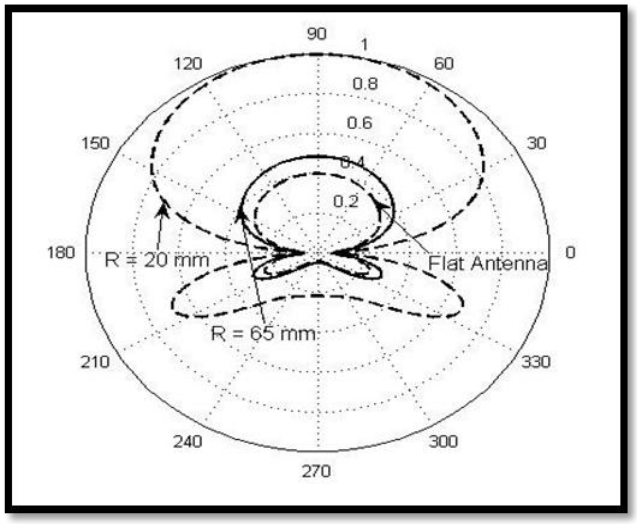

Figure 6. Normalized magnetic field for radius of curvatures 20, 65 mm and a flat antenna at θ=0:2π and φ=0^0.

As shown in Table 1, the resonance frequency and the total quality factor are increased with decreasing the curvature of microstrip printed antenna. The efficiency and the gain are increased with decreasing resonance frequency. The efficiency at radius of curvature 10 mm is 95.45% and decreased to be 95.12% at radius of curvature 50 and 93.59% at 200 mm, while the efficiency is 90.37% for a flat antenna. According to that result, the gain, for 10 and 50 mm is 5.43 dB and 5.34 dB respectively, while the gain is 4.6 dB for 200 mm and 1.48 dB for a flat antenna.

Increasing the quality factor with decreasing the curvature is due to the decreasing of the radiated power from the antenna. So, the efficiency will decreased with increasing the quality factor, due to decreasing in the radiated power, and the same for the gain.

Table 1. Resonance frequency, quality factor, efficiency, and gain for TM_{01} RT/duroid-5880 PTFE substrate

R	f_r (GHz)	Q_{tot}	η	G(dB)
Flat	2.1605	1239.824	90.37	1.48
200 mm	2.1601	1239.337	93.59	4.61
50 mm	2.159	1239.187	95.12	5.34
10 mm	2.1544	1238.494	95.45	5.43

5.2 K-6098 Teflon/Glass Substrate

The normalized electric field for K-6098 Teflon/Glass substrate is given in Figure 7 at different radius of curvatures 20, 65 mm and for a flat microstrip printed antenna.

Normalized electric field is calculated at θ equal to values from zero to 2π and φ equal to zero. At radius of curvature 20 mm, the radiation pattern of normalized electric field is wider than 65 mm and flat antenna, radiation pattern angle is almost 120^0, and gives a high value of electric field strength due to effective dielectric constant.

The normalized magnetic field is given in Figure 8, for the same conditions of normalized electric field. Normalized magnetic field is wider than normalized electric field for 20 mm radius of curvature; it is almost 170^0 for 20 mm radius of curvature. So, for normalized electric and magnetic fields, the angle of transmission is increased as a radius of curvature decreased.

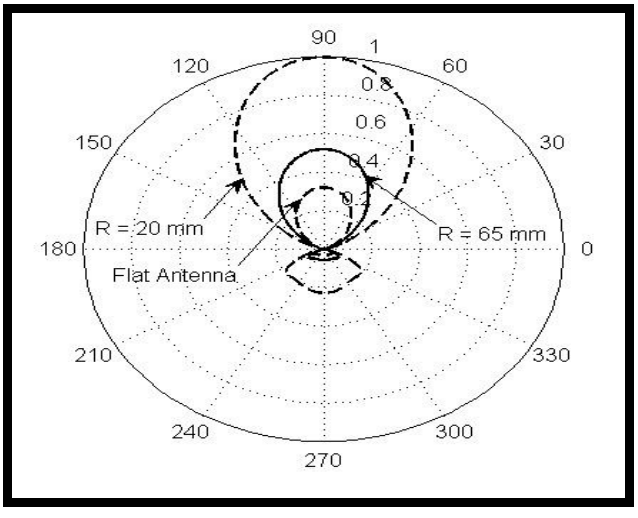

Figure 7. Normalized electric field for radius of curvatures 20, 65 mm and a flat antenna at θ=0:2π and φ=0^0.

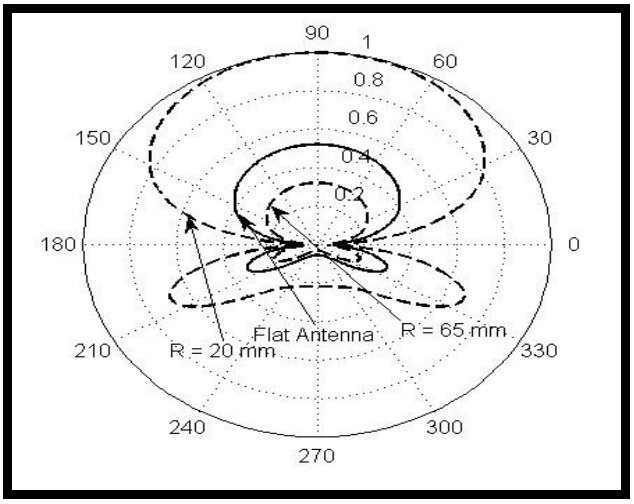

Figure 8. Normalized magnetic field for radius of curvatures 20, 65 mm and a flat antenna at θ=0:2π and φ=0^0.

The resonance frequency is increased with decreasing the curvature of microstrip printed antenna, as shown in Table 2. The total quality factor is decreased with increasing radius of curvature 10, 50, 200 mm, and for a flat antenna. The efficiency and gain have an opposite behavior with increasing radius of curvature. This disturbance in the behavior can be noticed in the normalized electric and magnetic fields with different resonance frequencies. The small radius of curvature gives a high gain and efficiency for a higher radiation angle and more broadened electric and magnetic field patterns.

Table 2. Resonance frequency, quality factor, efficiency, and gain for TM_{01} for K-6098 Teflon/Glass substrate

R	f_r (GHz)	Q_{tot}	η	G(dB)
Flat	0.96496	634.3995	85.33	1.48
200 mm	0.96483	633.06336	90.207	3.18
50 mm	0.96448	632.4919	90.37	5.85
10 mm	0.96299	632.11921	92.183	6.43

5.3 Epsilam-10 Ceramic-Filled Teflon

Normalized electric field for different radius of curvatures is illustrated in Figure 9. Normalized electric field is plotted for θ from zero to 2π and φ equal to zero. As the radius of curvature is decreasing, the radiated electric field is getting wider, so electric field at 20 mm radius of curvature is wider than 65 mm and 65 mm is wider than flat antenna. Electric field strength is increasing with decreasing the radius of curvature, because a magnitude value of the electric field is depending on the effective dielectric constant and the effective dielectric constant depending on the radius of curvature which decreases with increasing the radius of curvature.

Normalized magnetic field is wider than normalized electric field, and also, it is increasing with deceasing radius of curvature. Obtained results are at for θ from zero to 2π and φ equal to zero and for radius of curvature 20, 65 mm and for a flat microstrip printed antenna are shown in Figure 10.

For different radius of curvature, the resonance frequency changes according to the change in curvature, so the given normalized electric and magnetic fields are calculated for different resonance frequency according to radius of curvatures.

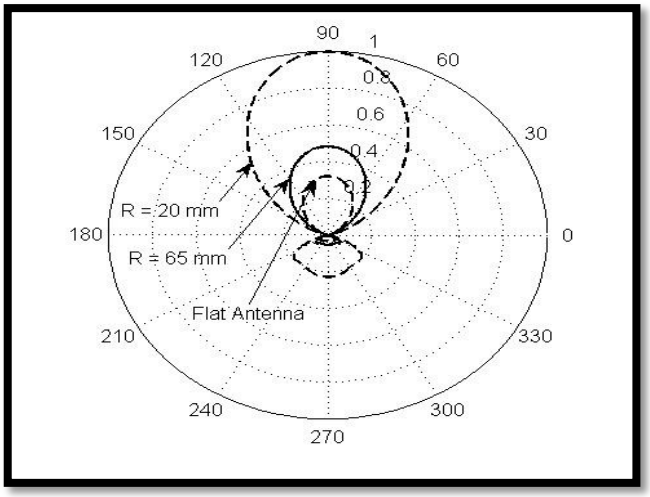

Figure 9. Normalized electric field for radius of curvatures 20, 65 mm and a flat antenna at θ=0:2π and φ=0^0.

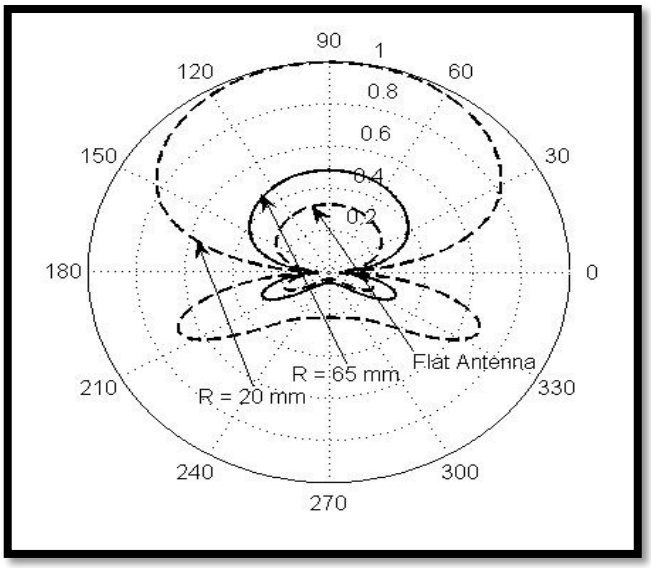

Figure 10. Normalized magnetic field for radius of curvatures 20, 65 mm and a flat antenna at θ=0:2π and φ=0^0.

Table 3 shows the resonance frequency, quality factor, efficiency, and gain for TM_{01} mode. The maximum efficiency obtained at radius of curvature 10 mm is 94.93% and maximum gain is 5.43 dB is also at 10 mm radius of curvature.

Table 3. Resonance frequency, quality factor, efficiency, and gain for TM_{01} Epsilam-10 ceramic-filled Teflon substrate

R	f_r (GHz)	Q_{tot}	η	G(dB)
Flat	1.9391	1043.14146	89.35	1.48
200 mm	1.9388	1042.44355	90.39	3.18
50 mm	1.9379	1042.3218	94.585	5.34
10 mm	1.9340	1041.988	94.93	5.43

6. Conclusion

The effect of curvature on the performance of conformal microstrip antenna on cylindrical bodies for TM_{10} mode is studied in this paper. Curvature affects the fringing field and fringing field affects the antenna parameters. The Equations for resonance frequency, gain, efficiency and quality factor as a function of curvature is introduced in this paper. These parameters are given for TM_{01} mode and using three different substrate materials RT/duroid-5880 PTFE, K-6098 Teflon/Glass and Epsilam-10 ceramic-filled Teflon.

For the three dielectric substrates, the decreasing in resonance frequency due to increasing in the curvature leads to decreasing in quality factor and on the other hand, leads to increasing in the efficiency and the gain of the microstrip printed antenna. The radiation pattern for electric and magnetic fields due to increasing in curvature is also increased and be more wider.

REFERENCES

[1] Heckler, M.V., et al., CAD Package to Design Rectangular Probe-Fed Microstrip Antennas Conformed on Cylindrical Structures. roceedings of the 2003 SBMO/IEEE MTT-S International, Microwave and Optoelectronics Conference, p p. 747-757, 2003.

[2] Q. Lu, X. Xu, and M. He, Application of Conformal FDTD Algorithm to Analysis of Conically Conformal Microstrip Antenna. IEEE International Conference on Microwave and Millimeter Wave Technology, ICMMT. , April 2008. p p. 527 – 530, 2008.

[3] Wong, K.L., Design of Nonplanar Microstrip Antennas and Transmission Lines. John & Sons, Inc, 1999.

[4] Josefsson, L. and P. Persson, Conformal Array Antenna Theory and Design 1ed. Wiley-IEEE Press, 2006.

[5] Thomas, W., R.C. Hall, and D. I. Wu, Effects of curvature on the fabrication of wraparound antennas IEEE International Symposium on Antennas and Propagation Society, pp. 1512-1515, 1997.

[6] J. Byun, B. Lee, and F.J. Harackiewicz, FDTD Analysis of Mutual Coupling between Microstrip Patch Antennas on Curved Surfaces. IEEE International Symposium on Antennas and Propagation Society, pp. 886-889, 1999.

[7] Balanis, C.A., AntennaTheory. New York: John Wiley & Sons, 2005.

[8] Pozar, D., Microstrip Antennas. IEEE Antennas and Propagation Proceeding, 1992.

[9] Krowne, C.M., Cylindrical-Rectangular Microstrip Antenna. IEEE Trans. on Antenna and Propagation, AP-31: pp. 194-199, 1983.

[10] Q. Wu, M. Liu, and Z. Feng, A Millimeter Wave Conformal Phased Microstrip Antenna Array on a Cylindrical Surface. IEEE International Symposium on Antennas and Propagation Society, pp. 1-4, 2008.

[11] J. Ashkenazy, S. Shtrikman, and D. Treves, Electric Surface Current Model for the Analysis of Microstrip Antennas on Cylindrical Bodies. IEEE Trans. on Antenna and Propagation, AP-33: pp. 295-299, 1985.

[12] K. Luk, K. Lee, and J. Dahele, Analysis of the Cylindrical-Rectangular Patch Antenna. IEEE Trans. on Antenna and Propagation. 37: pp. 143-147, 1989.

[13] S. Lei, et al., Anti-impact and Over-loading Projectile Conformal Antennas for GPS,. EEE 3rd International Workshop on Signal Design and Its Applications in Communications, pp. 266-269, 2007.

[14] Kolev, N.Z., Design of a Microstip Conform GPS Patch Antenna. IEEE 17th International Conference on Applied Electromagnetic and Communications, pp. 201-204, 2003

[15] A. Elrashidi, K. Elleithy, and Hassan Bajwa, "The Fringing Field and Resonance Frequency of Cylindrical Microstrip Printed Antenna as a Function of Curvature," International Journal of Wireless Communications and Networking (IJWCN), Jul.-Dec., 2011.

[16] A. Elrashidi, K. Elleithy, and Hassan Bajwa, "Effect of Temperature on the Performance of a Cylindrical Microstrip Printed Antenna for TM_{01} Mode Using Different Substrates," International Journal of Computer Networks & Communications (IJCNC), Jul.-Dec., 2011.

[17] A. Elrashidi, K. Elleithy, and Hassan Bajwa, "The Performance of a Cylindrical Microstrip Printed Antenna for TM_{10} Mode as a Function of Temperature for Different Substrates," International Journal of Next-Generation Networks (IJNGN), Jul.-Dec., 2011.

[18] S. M. Wentworth, Applied Electromagnetics, John Wiley & Sons, Sons, New York, 2005.

[19] R. F. Richards, Time-Harmonic Electromagnetic Fields, New York: McGraw-Hill, 1961.

[20] C. Balanis, Advanced Engineering Electromagnetic, John Wiley & Sons, New York, 1989.

[21] R. Garg, P. Bhartia, I. Bahl, and A. Ittipiboon, Microstrip Antenna Design Handbook, Aetech House, Boston, 2001